Environmental Science & Technology

pubs.acs.org/est

Article

Disproportionate Carbon Dioxide Efflux in Bacterial Metabolic Pathways for Different Organic Substrates Leads to Variable Contribution to Carbon-Use Efficiency

Caroll M. Mendonca, Lichun Zhang, Jacob R. Waldbauer, and Ludmilla Aristilde*

Cite This: *Environ. Sci. Technol.* 2024, 58, 11041−11052

Read Online

ACCESS | Metrics & More | Article Recommendations | Supporting Information

ABSTRACT: Microbial organic matter turnover is an important contributor to the terrestrial carbon dioxide (CO_2) budget. Partitioning of organic carbons into biomass relative to CO_2 efflux, termed carbon-use efficiency (CUE), is widely used to characterize organic carbon cycling by soil microorganisms. Recent studies challenge proposals of CUE dependence on the oxidation state of the substrate carbon and implicate instead metabolic strategies. Still unknown are the metabolic mechanisms underlying variability in CUE. We performed a multiomics investigation of these mechanisms in *Pseudomonas putida*, a versatile soil bacterium of the Gammaproteobacteria, processing a mixture of plant matter derivatives. Our ^{13}C-metabolomics data captured substrate carbons into different metabolic pathways: cellulose-derived sugar carbons in glycolytic and pentose-phosphate pathways; lignin-related aromatic carbons in the tricarboxylic acid cycle. Subsequent ^{13}C-metabolic flux analysis revealed a 3-fold lower investment of sugar carbons in CO_2 efflux compared to aromatic carbons, in agreement with reported substrate-dependent CUE. Proteomics analysis revealed enzyme-level regulation only for substrate uptake and initial catabolism, which dictated downstream fluxes through CO_2-producing versus biomass-synthesizing reactions. Metabolic partitioning as shown here explained the substrate-dependent CUE calculated from reported metabolic flux analyses of other bacteria, further supporting a metabolism-guided perspective for predicting the microbial conversion of accessible organic matter to CO_2 efflux.

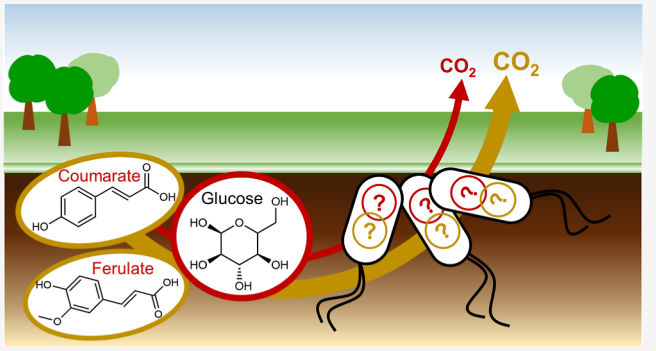

KEYWORDS: *metabolomics, carbon metabolism, carbon-use efficiency, lignocellulose, metabolic flux analysis*

1. INTRODUCTION

Model predictions of terrestrial carbon dioxide (CO_2) budgets depend critically on parameters that can adequately capture organic matter conversion by soil microorganisms (1). Therefore, understanding and predicting CO_2 efflux from microbial conversion of soil organic matter have become widespread endeavors in both field-scale and laboratory studies. Stable-isotope probing (SIP) is widely used to trace microbial activity in fields or soil microcosms after introducing a labeled substrate[2−5] and monitoring labeled fractions in CO_2, the biomass,[5,6] DNA,[5] or phospholipid-derived fatty acids.[2] Of particular interest in studies of soil microbial ecology is the determination of microbial carbon-use efficiency (CUE), which refers to the fractional partitioning of consumed organic substrates to biomass; the remaining fraction (i.e., 1-CUE) represents the sum of CO_2 efflux and metabolite release.[6,7] Therefore, using SIP experiments, the CUE is generally determined either directly by accounting for labeled biomass content[8] or indirectly based on the fraction of substrate carbon respired as CO_2.[6] While CUE measurements based solely on CO_2 efflux provide a valuable indicator, it may not capture the full spectrum of carbon losses, which can include metabolite secretions. A global CUE study across 98 sites reported a substrate dependence of microbial CUE whereby median CUE value was higher for the sugar glucose (0.63−0.73) than for organic acids (<0.4) or plant residues (<0.3).[9] Understanding the driver of microbial CUE is of particular interest to disentangle the role of microbes in the global carbon cycle. However, the underlying microbial strategies responsible for this range in substrate-specific CUE (ssCUE) represent an important knowledge gap in microbial ecology that remains unresolved. There are two main proposed biochemical reasons for the observed variability in ssCUE:[9−11] first, that the different substrates would require different catabolic pathways

Received: February 4, 2024
Revised: May 18, 2024
Accepted: May 22, 2024
Published: June 11, 2024

https://doi.org/10.1021/acs.est.4c01328
Environ. Sci. Technol. 2024, 58, 11041−11052

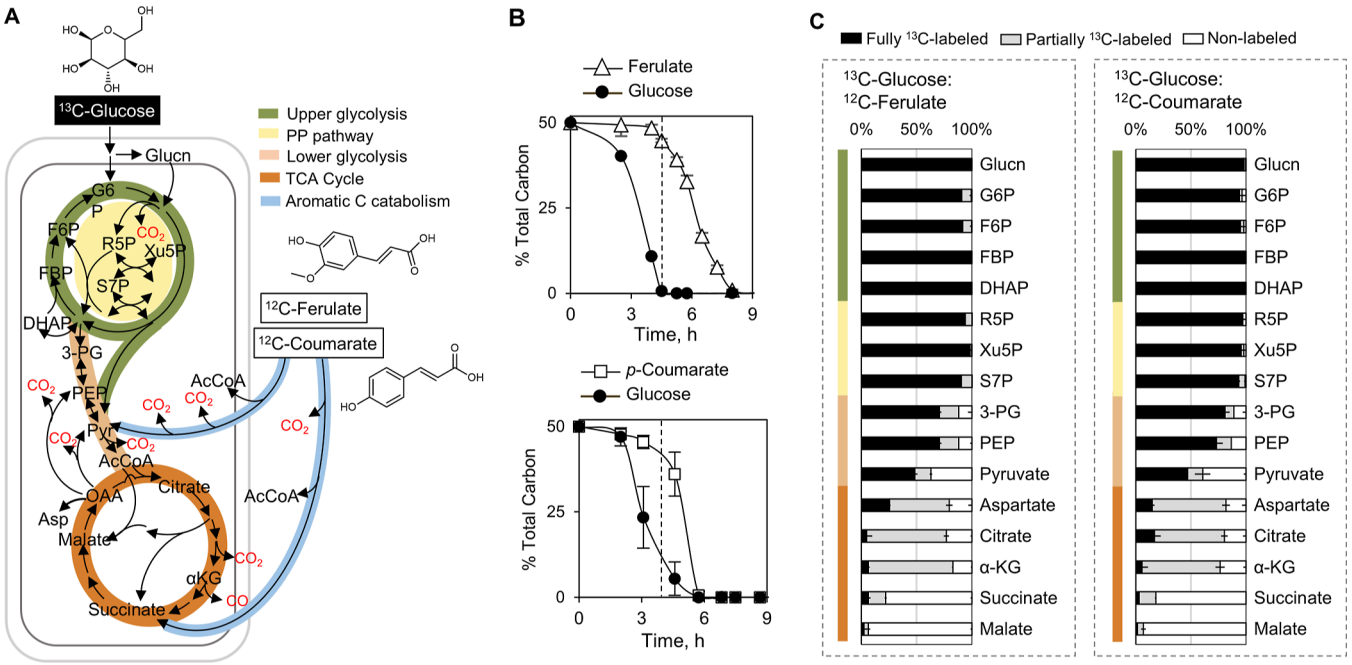

Figure 1. (A) Schematic overview of metabolic pathways for catabolism of glucose, ferulate, and *p*-coumarate showing metabolic reactions (black arrows) in upper glycolysis (green), PP pathway (yellow), lower glycolysis pathway (light orange), the TCA cycle (dark orange), and aromatic carbon (C) metabolism (blue); only the names of the measured metabolites are shown. (B) Kinetics of substrate depletion (in % of total carbon) in *P. putida* mt-2 cultures grown on a 1:1 carbon equivalent mixture of (top) glucose/ferulate or (bottom) glucose/*p*-coumarate. (C) Intracellular metabolite labeling after assimilation of (left) [U−$^{13}C_6$]-glucose and unlabeled ferulate or (right) [U−$^{13}C_6$]-glucose and unlabeled *p*-coumarate in *P. putida* mt-2: fully ^{13}C-labeled (black), partially ^{13}C-labeled (gray), and nonlabeled (white). Error bars in B and C represent standard deviation values (n = 3 biological replicates).

that result in different utilization efficiencies;[10,11] second, that substrates with a higher nominal oxidation state of carbon (NOSC) due to higher chemical energy per unit mol of carbon would result in a higher ssCUE.[10,12,13] Recent studies found no correlation between NOSC and substrate-specific assimilation for soil fungal and bacterial isolates consuming a mixture of different organic compounds.[14,15] Therefore, metabolic pathways involved in microbial processing of different organic substrates have been proposed to underlie reported variations in substrate utilization for biomass synthesis.[15−19]

Here, we sought to probe how *Pseudomonas putida*, a soil bacterium with diverse metabolic capabilities, would process the metabolism of a mixture of representative lignocellulose-related compounds toward CO_2 versus biomass. More than 50% of soil organic matter is derived from plant matter, including lignocellulose.[20] Lignocellulose, the most abundant biopolymer on earth, is composed of two carbohydrate polymers, cellulose (9−80%) and hemicellulose (10−50%), and lignin (5−35%), a heteropolymer of aromatic units.[21,22] Cellulose and hemicellulose, both of which are polymers of sugars, can be easily metabolized by soil microbes, but lignin is considered highly recalcitrant to biodegradation.[23] However, several bacteria and fungi produce extracellular oxidative enzymes that can depolymerize lignin, thereby providing lignin derivatives for further metabolism by a subset of microbes with pathways for aromatic carbon catabolism.[24−26] Pseudomonas species, which represent important members of the Gammaproteobacteria widely present in soil microbial communities,[27,28] are able to metabolize sugars as well as lignin-related aromatic derivatives such as *p*-coumarate, ferulate, vanillate, and 4-hydroxybenzoate.[29−31] Therefore, given the ubiquity and metabolic versatility of Pseudomonas species, they present ideal candidate species for probing the bacterial metabolism underlying the ssCUE of lignocellulose-related compounds.

The objective of the present study was to address the knowledge gap regarding the metabolic underpinnings of ssCUE using *P. putida* mt-2, a widely studied soil bacterial isolate, processing a mixture containing ferulate or *p*-coumarate as a lignin-related aromatic compound and glucose from cellulose, both of which are substrates potentially available to microbes in soils (Figure 1A). After initial assimilation of a sugar or an aromatic substrate, the substrate carbons are expected to route throughout the network of central carbon metabolism to meet carbon demands for biomass biosynthesis. On the one hand, following uptake of glucose or other six-carbon sugar substrates, the assimilated carbons would enter first through upper glycolysis and subsequently feed the pentose-phosphate (PP) pathway required for ribonucleotide biosynthesis and downstream into lower glycolysis and the tricarboxylic acid (TCA) cycle to support amino acid biosynthesis (Figure 1A). On the other hand, carbons following cleavage of aromatic substrates would first enter the TCA cycle and, through cataplerotic reactions that convert TCA cycle intermediates to metabolites in lower glycolysis, carbon fluxes are subsequently subjected to gluconeogenesis, the reverse of glycolysis, to provide metabolite precursors to biomass biosynthesis in upper glycolysis and the PP pathway (Figure 1A). As illustrated in Figure 1A, fluxes through the different pathways in the metabolic network involve the production of carbon dioxide (CO_2). Therefore, we hypothesized that the distinct routing of each assimilated substrate into pathways with a relatively different number of CO_2-producing versus biomass-generating reactions would dictate the ssCUE values.

https://doi.org/10.1021/acs.est.4c01328
Environ. Sci. Technol. 2024, 58, 11041−11052

To test this hypothesis, we conducted a multi-omics study involving ^{13}C-assisted metabolomics, proteomics, and fluxomics to evaluate the metabolic network responsible for the contribution of the carbons from the different lignocellulose derivatives to CO_2-generating and biomass-synthesizing metabolic reactions. First, we employed long-term isotopic enrichment using ^{13}C-labeled glucose with nonlabeled aromatic substrates to determine the allocation of each substrate type into different pathways in central carbon metabolism. Second, using ^{13}C-metabolic flux analysis, we determined the carbon flux contribution from each substrate in the mixture toward metabolic reactions involved in CO_2 efflux and ssCUE. Third, we monitored changes in protein levels in cells fed on a mixture of glucose with an aromatic compound relative to cells fed on only glucose to distinguish between metabolite-level and protein-level regulation. While bulk CO_2 data are widely used to monitor microbial respiration during substrate conversion to CO_2,[6] these data do not provide any information about substrate-specific contribution to CO_2 during microbial processing of a mixture. Such substrate-specific information would require the measurement of the isotopic distribution of the bulk CO_2 derived from the metabolism of a mixture with ^{13}C-labeled and nonlabeled substrates as demonstrated previously.[19] However, in the absence of data on intracellular metabolite labeling patterns, the latter data would still not capture explicitly the metabolic pathways responsible for the CO_2 efflux, albeit hypothetical frameworks regarding CO_2 production from the underlying metabolic network can be deduced.[19] Assimilation of position-specific ^{13}C-labeled glucose into phospholipid fatty acid as a representative biomass derivative was employed previously to estimate metabolic pathways involved,[18] but complex deconvolution of isotopomer data was required to associate the specific labeling of the fatty acid to flux through different metabolic pathways. Such data deconvolution performed with a single substrate would be challenging to implement to capture specific pathway contributions in ssCUE during the assimilation of substrate mixtures. Here, our application of ^{13}C-metabolomics profiling coupled with metabolic flux analysis overcomes the limitations of bulk CO_2 data by leveraging direct annotation of intracellular metabolites in the central carbon metabolism to gain substrate-specific and pathway-specific insights on CUE. Taken together, we present a roadmap for coupling the considerations of metabolic pathways with the application of SIP in tracking the conversion of bioavailable substrates from soil organic matter mixtures into CO_2 and biomass synthesis by soil microorganisms.

2. MATERIALS AND METHODS

2.1. Cell Culturing and Nutrient Conditions. The bacterial strain,*P. putida* mt-2, was acquired from ATCC (American Type Culture Collection, Manassas, VA) and stored at −80 °C in nutrient-rich liquid Luria−Bertani medium and 25% glycerol. Unless mentioned otherwise, all chemicals for standards and growth media were purchased from MilliporeSigma (St. Louis, MO) or Fisher Scientific (Pittsburgh, PA). Carbon source-specific growth experiments were conducted in 125 or 250 mL baffled flasks, with cell suspensions not exceeding one-fifth of the total flask volume in an incubator shaker (model I24; New Brunswick Scientific, Edison, NJ) at 30 °C and 220 rpm. The pH-adjusted (pH 7.0) and filter-sterilized (0.22 μm nylon; Waters) minimal medium contained the carbon substrates; a 1:1 mixture of glucose/*p*-coumarate or glucose/ferulate at a total concentration of 100 mM C; the following major nutrient salts: 5.0 mM NaH_2PO_4, 20 mM K_2HPO_4, 37 mM NH_4Cl, 17 mM NaCl, 0.81 mM $MgSO_4{\cdot}7H_2O$, and 34 μM $CaCl_2{\cdot}2H_2O$; and the following trace metal nutrients: 30 μM $FeSO_4{\cdot}7H_2O$, 0.86 μM CuSO4·5H2O, 1.9 μM H_3BO_3, 7.7 μM $ZnSO_4{\cdot}7H_2O$, 0.75 μM $MnSO_4{\cdot}5H_2O$, 0.26 μM $NiCl_2{\cdot}6H_2O$, and 0.31 μM $Na_2MoO_4{\cdot}5H_2O$. As references for the proteomic analysis, growth experiments were conducted with glucose-only as the only carbon source (100 mM C total). To achieve cellular acclimation in each nutrient condition, all experiments were conducted following two transfers into a minimal-nutrient medium supplemented with the carbon source during the exponential growth phase. Additionally, cells were washed with the minimal-nutrient medium between transfers to remove the extracellular matrix from the previous culture. Biomass growth was monitored by measuring the optical density at 600 nm (OD_{600}) using an Agilent Cary UV−visible spectrophotometer (Santa Clara, California). Exponential growth rate (h^{-1}) was determined via regression analysis. Measurement of cell dry weight in grams (gCDW) as a function of exponential OD_{600} was obtained following lyophilization of sample aliquots (1.5 mL) using a Labconco (Kansas City, MO, USA) Freeze-Dryer System.

2.2. Extracellular Substrate Depletion. To determine substrate depletion by the cells, 0.5 mL culture aliquots of three biological replicates were harvested periodically throughout growth and pelleted with 5 min of centrifugation at 9391 g and 4 °C (Centrifuge 5423 R, Eppendorf, Hauppauge, NY). The supernatant was removed, filtered (Costar Spin-X 0.22 μM filters), and stored at −20 °C until instrumental analysis. Standards for glucose, ferulate, and *p*-coumarate were prepared in minimal nutrient media.

Ferulate and *p*-coumarate were quantified using ultrahigh-performance liquid chromatography (UHPLC) with UV detection at 275 nm (Thermo Scientific Vanquish Flex with diode array detector) using a reversed-phase C18 column (ZORBAX Eclipse Plus, 4.6 × 100 mm, 5 μm; Agilent) maintained at 25 °C with a guard column (4.6 × 12.5 mm, 5 μm; Agilent). The method demonstrated by Hefni et al.[32] for separating phenolic acids was modified to a total run time of 18 min at a flow rate of 0.9 mL min^{-1} and injection volume of 10 μL. The mobile phases consisted of 1% formic acid in LC−MS grade water (solvent A) and 80:10:10 v/v acetonitrile/methanol/LC−MS grade water (solvent B). For solvent B, a multistep gradient was used: 0 min, 6%; 1 min, 6%; 8.5 min, 25% B; 9 min, 25%; 9.5 min, 6%; 10.5 min, 6%.

Glucose was quantified using a UHPLC system (Thermo Fisher Scientific DionexUltiMate 3000, Waltham, MA, USA) coupled to a high-resolution accurate-mass mass spectrometer (Thermo Fisher Scientific Q Exactive quadrupole-Orbitrap hybrid MS) with ESI operating in negative mode as described previously.[33] Chromatographic separation was performed using a XBridge Amide column (Waters, Milford, MA) with dimensions of 4.6 × 100 mm and a particle size of 3.5 μm; a column temperature of 25 °C was used. The volume injected was 10 μL of samples prepared in 50% v/v ACN at a flow rate of 0.8 mL min^{-1}. The mobile phases consisted of 100% ACN with 0.05% v/v triethylamine (solvent A) and 50:50 v/v isopropyl alcohol/LC−MS water with 0.05% v/v triethylamine (solvent B). A multistep gradient was used for solvent A: 0 min, 90%; 12 min, 90%; 12.05 min, 60%; 17 min, 60%; 19.05 min, 40%; 25 min, 20%; 26.05 min, 90%; 30.5 min, 90%.

https://doi.org/10.1021/acs.est.4c01328
Environ. Sci. Technol. 2024, 58, 11041−11052

2.3. Intracellular ^{13}C Labeling. To monitor the intracellular assimilation of substrates, we performed ^{13}C-metabolomics profiling of the cells grown on [U−$^{13}C_6$]-glucose with either unlabeled *p*-coumarate or unlabeled ferulate. Labeled substrates were purchased from Cambridge Isotopes (Tewksbury, MA, USA). To ensure long-term intracellular labeling, liquid cultures were grown for at least two doubling times in their respective medium solutions. Cell suspensions were harvested after two transfers into a minimal-nutrient medium containing the aforementioned labeled substrates; washing with minimal-nutrient medium was performed between the transfers. During exponential growth, cell suspensions were filtered, and cell-containing filters were immediately quenched in a 2 mL solution of methanol/acetonitrile/water (40:40:20) maintained at 4 °C. Solutions with the lysed cells were subsequently filter-centrifuged (Sigma-Aldrich Spin-X, 0.22 μM filters), and aliquots of the supernatants were dried under nitrogen gas. Prior to analysis via LC−MS, dried aliquots were resuspended in ultrapure LC−MS grade water (Fisher Scientific). Following analysis and identification of intracellular metabolites by LC-HRMS, ^{13}C-labeling fractions were extracted with the Metabolomic Analysis and Visualization Engine (MAVEN) software[34] and were then corrected for natural ^{13}C abundance.

2.4. Metabolomics Analysis via LC−MS. Both intracellular and extracellular metabolites were analyzed by a reversed-phase ion-pairing method via ultrahigh-performance LC (UHPLC; Thermo Scientific DionexUltiMate 3000) coupled to a high-resolution accurate-mass mass spectrometer (Thermo Scientific Q Exactive) with electrospray ionization operated in full-scan negative mode (m/z range 70−900) as described previously.[35] A Waters Acquity UPLC BEH C18 1.7 μm with a column size of 2.1 × 100 mm (Waters Corporation, Massachusetts) was used and maintained at 25 °C throughout the run. Solvent A contained 97:3 v/v LC−MS grade water/methanol with acetic acid (15 mM) and tributylamine (10 mM), and solvent B contained 100% methanol. The total run time was 25 min, with a flow rate of 180 μL min^{-1} and a sample injection volume of 10 μL. A multistep gradient for solvent A was used: 0 min, 100%; 2.5 min, 100%; 5 min, 80%; 7.5 min, 80%; 10 min, 45%; 12 min, 45%; 14 min, 5%; 17 min, 5%; 18 min, 0%; 25 min, 0%. The following metabolites were monitored: gluconate, 6-phosphogluconate (6 PG), glucose-6-phosphate (G6P), fructose-6-phosphate (F6P), fructose-1,6-bisphosphate (FBP), dihydroxyacetone-phosphate (DHAP), ribose-5-phosphate (R5P), xylulose-5-phosphate (Xu5P), sedoheptulose-7-phosphate (S7P), phosphoenolpyruvate (PEP), 3-phosphoglycerate (3 PG), pyruvate, α-ketoglutarate (α-KG), citrate, aspartate, succinate, and malate. Aspartate labeling was taken as a surrogate for oxaloacetate (OAA) labeling due to the direct synthesis of aspartate from OAA.[36]

To monitor metabolite secretion rates, quantification of metabolites in the extracellular medium was conducted during the exponential phase. Culture aliquots (0.5 mL) were harvested, subjected to centrifugation (9391 g and 4 °C for 5 min), and subsequently filtered (0.22 μM filters). The resulting supernatant was then analyzed by using LC−MS as described above. Metabolite excretion rates (in mol C g_{CDW}^{-1} h^{-1}) were determined by regression analysis.

2.5. Metabolic Flux Analysis. Metabolic flux analysis of the central carbon metabolism was performed using software 13CFLUX2[37] and constrained on the following experimental data: substrate consumption rate, metabolite secretion rates, growth rate, and genome-scale cellular stoichiometry.[36] Both the sequence of the TOL plasmid pWW0 of *P. putida* mt-2[38] and the sequence of the chromosome of *P. putida* mt-2 have been reported; the chromosomal sequence is that of *P. putida* KT2440,[39] the plasmid-less strain derived from *P. putida* mt-2. Therefore, the well-characterized stoichiometry data available for *P. putida* KT2440 was used in our metabolic flux analysis of *P. putida* mt-2. Specifically, we used the biomass experimentally determined growth rates and published biomass composition of *P. putida* KT2440;[40] carbon efflux rates were calculated for carbon routing toward the biosynthesis of proteins, nucleic acids, and cell membrane. The initial flux values were set based on published values[36,41] and subsequently optimized based on the experimental observations. The quality of the fit to experimental data was measured by calculating the sum of squared residuals based on comparisons of model-estimated metabolite labeling patterns to the measured values.[42]

2.6. Calculation of Carbon Utilization Efficiency. As we stated in the Introduction, in lieu of monitoring bulk CO_2 data to infer CUE, we aim to employ a ^{13}C-metabolomics approach to directly determine substrate assimilation for our CUE calculations. Specifically, following feeding on [U−$^{13}C_6$]-glucose with unlabeled *p*-coumarate, we obtained ^{13}C fractional labeling data of metabolites to determine the relative contribution of the individual substrates toward the CO_2 produced in a particular metabolic reaction or toward a particular biomass precursor. Metabolites of interest for CO_2 efflux include 6 PG, OAA, pyruvate, isocitrate, and α-KG; metabolites of interest for biomass efflux include G6P, DHAP, erythrose-4-phosphate (E4P), 3 PG, PEP, pyruvate, and OAA. Metabolite labeling of R5P and aspartate was used to approximate the labeling of E4P and OAA, respectively.

Using the mass distribution vector, we determined the fractional contribution (FC) of each of the substrates to biomass precursor metabolites or relevant metabolites produced from decarboxylation reactions (i.e., paired with CO_2 production) based on the following equation[43]

$$\mathrm{FC} = \frac{\sum_{i=0}^{n} iS_i}{n} \tag{1}$$

In eq 1, n is the number of carbon atoms in the resulting metabolite, i denotes the isotopologues, and S is the relative fraction of the isotopologues.[43] Next, using the FC of each substrate toward CO_2 efflux or biomass efflux, we calculated the ssCUE as reported previously[9,15]

$$\mathrm{CUE} = 1 - \frac{R + E}{U} \tag{2}$$

Here, R is the respiration rate (in mol C g_{CDW}^{-1} h^{-1}) from the individual assimilated substrate, E is the collective secretion rates of metabolites (in mol C g_{CDW}^{-1} h^{-1}), and U is the uptake rate (in mol C g_{CDW}^{-1} h^{-1}) of individual assimilated substrates. Of all of the monitored extracellular metabolites, only gluconate exhibited appreciable secretion from which a secretion rate was determined. Therefore, E refers here only to the gluconate secretion rate. Error was propagated by using standard deviations for R, E, and U.

2.7. Proteomics Methodology and Analysis. At midexponential phase (OD_{600} = 0.8−1), sample aliquots (25 mL) were harvested from biological replicates (n = 3), pelleted via centrifugation at 9391 g and 4 °C, separated from the

https://doi.org/10.1021/acs.est.4c01328
Environ. Sci. Technol. 2024, 58, 11041−11052

centrifuge, and stored at −80 °C until further analysis. These cell pellets were then extracted by heating and vertexing at 95 °C for 20 min in a reducing and denaturing buffer [SDS (1%)/Tris (200 mM, pH 8.0)/DTT (10 mM)] and with cysteine thiols alkylated with 40 mM iodoacetamide. Proteins were then purified by a modified eFASP (enhanced filter-aided sample preparation) protocol,[44] using Sartorius Vivacon 500 concentrators with a 30 kDa nominal cutoff. Proteins were digested with MS-grade trypsin (37 °C overnight), and peptides were eluted from the concentrator and dried via vacuum centrifugation. Peptides were then isotopically labeled at *N*- and *C*-termini using the diDO-IPTL methodology[45] for quantitative proteomic analysis. Briefly, *C*-termini were labeled with oxygen-16 or -18 by an enzymatic exchange in isotopic water of a >98 atom % enrichment, and *N*-termini were labeled with un- or dideuterated formaldehyde via reductive alkylation using sodium cyanoborohydride. Peptide extracts from each sample were split, and aliquots were labeled separately with $CD_2O/^{16}O$ and $CH_2O/^{18}O$; the latter were pooled to serve as a common internal standard for quantification. Aliquots of the ^{16}O-labeled peptides and ^{18}O-labeled internal standard were mixed 1:1 (v/v) and analyzed by LC−MS for protein expression quantification.

The peptide samples were then separated on a monolithic capillary C18 column (GL Sciences Monocap Ultra, 100 μm I.D. × 200 cm length) with a water−acetonitrile and 0.1% formic acid gradient (2−50% ACN over 180 min) at 360 nL min^{-1} using a Dionex Ultimate 3000 LC system with nanoelectrospray ionization (Proxeon Nanospray Flex source) for LC−MS analysis. Mass spectra were collected on an Orbitrap Elite mass spectrometer (Thermo) operating in data-dependent acquisition mode, with one high-resolution (120,000 $m/\Delta m$) MS1 parent ion full scan triggering 15 rapid-mode MS2 CID fragment ion scans of selected precursors. Proteomic mass spectral data were analyzed using MorpheusFromAnotherPlace (MFAP)[45] and the predicted proteome of *P. putida* mt-2 as search databases. Precursor and product ion mass tolerances for MFAP searches were set to 20 ppm and 0.6 Da, respectively. Static cysteine carbamidomethylation and variable methionine oxidation, *N*-terminal (d4)-dimethylation, and *C*-terminal $^{18}O_2$ were included as modifications. The false discovery rate for peptide-spectrum matches was controlled by target-decoy searching to <0.5%. Protein-level relative abundances and standard errors were calculated in *R* using the Arm postprocessing scripts for diDO-IPTL data.[45]

2.8. Statistical Analysis. For proteomics analysis, significantly differential protein expression between experimental conditions was determined by calculating a *Z*-score for protein abundance differences by taking the difference in the mean (log_2-transformed) protein abundance between conditions and dividing it by the sum of the total uncertain estimate for that protein under the two conditions. This total uncertainty estimate for a given condition was taken as the root-square sum of (1) the standard deviation of a protein's abundance across the biological replicates of that condition and (2) the average standard error of the protein's abundance across quantified spectra within each replicate. These *Z*-scores were converted to *p*-values by assuming a standard normal distribution. The familywise error rate for significantly differential expression between conditions was controlled to 0.05 using the *q*-value method to correct for multiple testing.[46]

All growth and metabolomics experiments were conducted on three biological replicates. Statistical analysis of CO_2 efflux across multiple CO_2-generating reactions was determined using one-way ANOVA followed by Tukey HSD posthoc tests. For comparisons between discriminate CUEs of substrates in mixtures, statistical analysis was conducted using a two-tailed unpaired *t*-test analysis. Statistically significant difference was determined at $p \leq 0.05$.

2.9. Data Availability. Proteomics MS data and metabolomics LC−MS data are freely available in the ProteomeXchange and MetaboLights depositories under identifiers PXD4041724 and MTBLS6373, respectively.

3. RESULTS AND DISCUSSION

3.1. Metabolic Routing of Assimilated Carbons from a Mixture of Lignocellulose-Related Substrate Types. Growth and metabolic experiments were conducted with *P. putida* mt-2 cultures grown on a 1:1 carbon-equivalent glucose:*p*-coumarate or glucose:ferulate mixture. Both substrate types were depleted simultaneously in each mixture scenario after approximately 50 to 75% of the glucose was already depleted (Figure 1B). Despite this seeming preference for glucose, there were near-equal carbon-equivalent consumption rates of both substrates (46.9 ± 7.8 mM C glucose g_{CDW}^{-1} h^{-1} and 54.0 ± 6.0 mM C *p*-coumarate g_{CDW}^{-1} h^{-1} for the glucose:*p*-coumarate mixture, and 51.7 ± 8.6 mM C glucose g_{CDW}^{-1} h^{-1} and 47.6 ± 5.3 mM C ferulate g_{CDW}^{-1} h^{-1} for the glucose:ferulate mixture) (Figure 1B; Supporting Information, Table S1). To monitor the intracellular incorporation of the lignocellulose-related substrates during the coconsumption phase, we performed ^{13}C-metabolomics profiling of the cells grown on [U−$^{13}C_6$]-glucose with either unlabeled *p*-coumarate or with unlabeled ferulate (Figure 1C; Supporting Information Tables S2 and S3). The fraction of ^{13}C labeling of metabolites captured the relative assimilation of the ^{13}C-labeled sugar carbons versus the nonlabeled carbons of the aromatic substrates into the different metabolic pathways.

Due to the lack of a 6-phosphofructokinase gene to convert F6P to FBP, the catabolism of glucose in *Pseudomonas* species relies on a cyclic carbon flux from the Entner−Doudoroff (ED) pathway, another forms of glycolysis, instead of the Embden−Meyerhof−Parnas (EMP) pathway, the traditional pathway of glycolysis; the ED pathway is linked to the EMP pathways to meet the required carbon flux demand for the PP pathway (Figure 1A).[41,47,48] We found that the metabolites involved in initial glucose catabolism [G6P and gluconate (Glucn)], upper glycolysis (F6P and FBP), the PP pathway (R5P, Xu5P, and S7P) were all dominated by glucose-derived ^{13}C carbons, thereby highlighting the lack of gluconeogenic flux of the aromatic substrates toward upper glycolysis and the PP pathway (Figure 1C). Metabolites in lower glycolysis (DHAP, 3 PG, and PEP) contained significant proportions of ^{13}C (>71%) derived from glucose accompanied by evidence of nonlabeled fractions from the gluconeogenic flux of the aromatic carbons (Figure 1C). Pyruvate, which represents a metabolic entry point following ring cleavage of ferulate or *p*-coumarate, was only up to 50% ^{13}C-labeled due to incorporation of nonlabeled carbons from the assimilated aromatic substrate subjected to gluconeogenic flux upstream of the TCA cycle (Figure 1C). Labeling of the TCA cycle metabolites further reflected the assimilation of carbons derived from both glucose and the aromatic substrates, with a clear preference for nonlabeled aromatic carbons (Figure

https://doi.org/10.1021/acs.est.4c01328
Environ. Sci. Technol. 2024, 58, 11041−11052

1C). Metabolites in the oxidative side of the TCA cycle (citrate and α-KG) contained nonlabeled (~20%), partially ^{13}C-labeled (~70%), and fully ^{13}C-labeled (10%) carbons whereby partially labeled fractions incorporated carbons derived from both ^{13}C-glucose and the nonlabeled aromatic substrate (Figure 1C). However, metabolites on the reductive side of the TCA cycle (malate and succinate) were predominately nonlabeled (>78%) (Figure 1C), due to the assimilation entry route for the aromatic compounds at the succinate node, which is followed downstream by malate in the canonical direction of the TCA cycle (Figure 1C). In sum, our ^{13}C-metabolomics data revealed a nonuniform partitioning of substrate carbons derived from glucose and lignin aromatics through different metabolic pathways. We obtained proteomics data to probe the regulatory mechanism that dictates this metabolic partitioning of the assimilated substrate carbons.

3.2. CO_2-Producing Metabolic Reactions in the TCA Cycle Are under Carbon Influx Regulation Rather Than Enzyme-Level Regulation. We evaluated changes in the protein levels in cells fed on a mixture of glucose and a lignin derivative (ferulate or *p*-coumarate) relative to feeding on glucose alone (Figure 2). Remarkably, between the mixture and glucose alone, there was no change in the abundances of any of the proteins involved in decarboxylation reactions in pathways in the central carbon metabolism, including the PP pathway, the cataplerotic reactions, lower glycolysis, and the TCA cycle (Figure 2; Supporting Information Table S4). By contrast, the abundances of several proteins involved in the uptake and initial catabolism of each substrate were found to be dependent on the growth conditions (Figure 2).

First, all proteins associated with the uptake transporter of the aromatic substrates and initial catabolism of these substrates to the aromatic intermediate protocatechuate were detected only in the cells fed on the mixture with both glucose and an aromatic substrate; these proteins were absent in the presence of glucose alone (Figure 2). In *P. putida* mt-2, there are three pathways for the cleavage of aromatic substrates (at the *meta*, *ortho*, or *para* position) encoded in the genome before subsequently routing the resulting carbon skeletons to the TCA cycle.[49,50] While the proteins in the *meta*-cleavage pathway were not identified in both growth conditions with the mixture, all the proteins in the *ortho*-cleavage pathways were detected in cells fed on the substrate mixtures, and only two of the eight proteins in the *para*-cleavage pathway were found in both the glucose alone and the lignocellulose-related mixture conditions (Figure 2). These data signified a prevalence of the *ortho*-cleavage pathway and the possible participation of the *para*-cleavage pathway for the initial aromatic substrate catabolism (Figure 2).

In initial glucose catabolism or upper glycolysis, the following relevant proteins were detected in cells grown on glucose alone or glucose with *p*-coumarate but absent in cells grown on glucose with ferulate: gluconate 2-dehydrogenase (GAD), 2-ketogluconate-6-phosphate reductase (KGUD), glucose-6-phosphate isomerase (PGI), and ribulose-phosphate 3-epimerase (RPE) (Figure 2). The absence of GAD and KGUD in cells grown on glucose with ferulate implied the lack of phosphorylation of the glucose oxidation product (2-ketogluconate) to 6-PG.[47] Furthermore, the absence of PGI and RPE implied, respectively, the lack of fluxes through upper EMP and the oxidative PP pathway, thereby emphasizing the operation of the ED pathway as the primary route for glycolysis in the presence of ferulate[47] (Figure 2). The abundance of

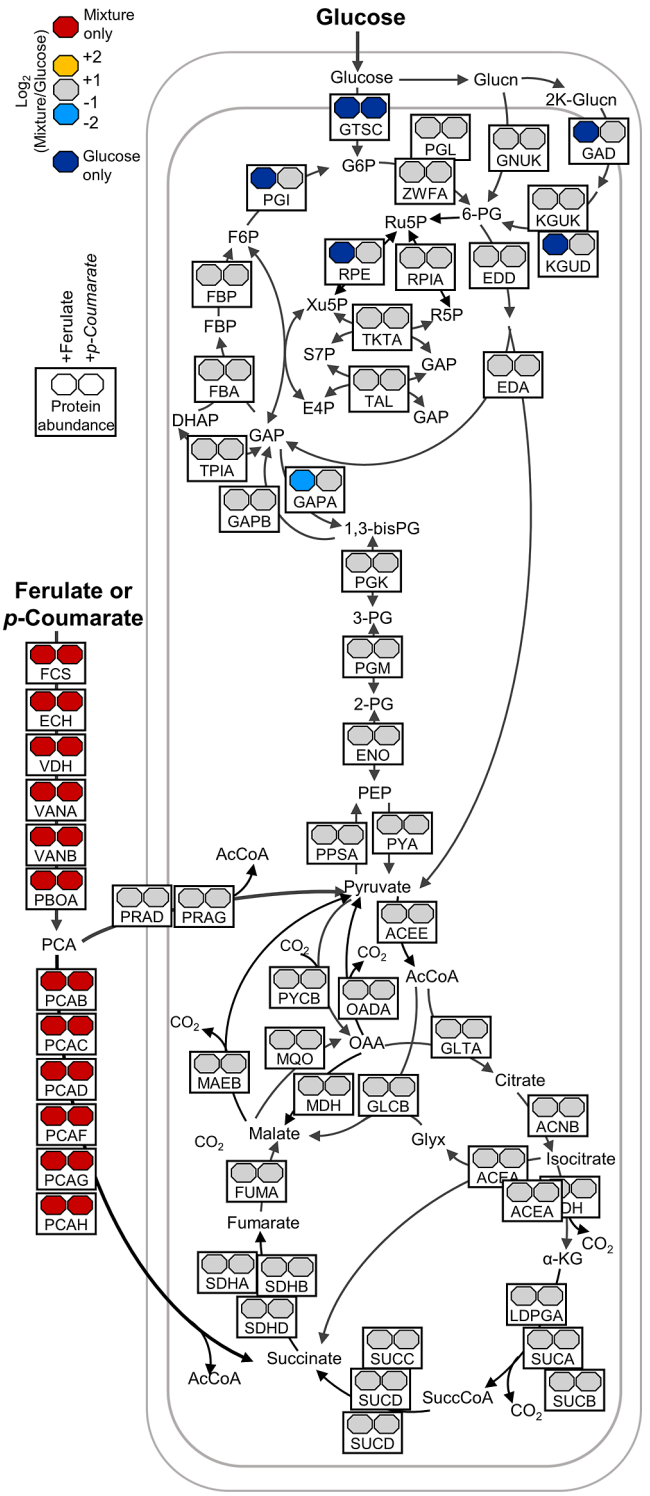

Figure 2. Log_2 fold changes in protein content of *P. putida* mt-2 cells grown on glucose/ferulate (left polygons) or glucose/*p*-coumarate (right polygons) relative to cells grown on control (glucose alone). Gray indicates proteins with no significant changes in levels between cells grown on the lignocellulose-related mixture and control, navy blue indicates proteins only detected in glucose-grown cells, and red indicates proteins only detected in cells grown on lignocellulose-related mixtures. Compared to cells grown on glucose, the increase and decrease in protein levels of cells grown on lignocellulose-related mixtures are shown with yellow and bright-blue colors, respectively. Data are obtained from four biological replicates (n = 4). Data and data statistics are provided in Supporting Information Table S4.

https://doi.org/10.1021/acs.est.4c01328
Environ. Sci. Technol. 2024, 58, 11041−11052

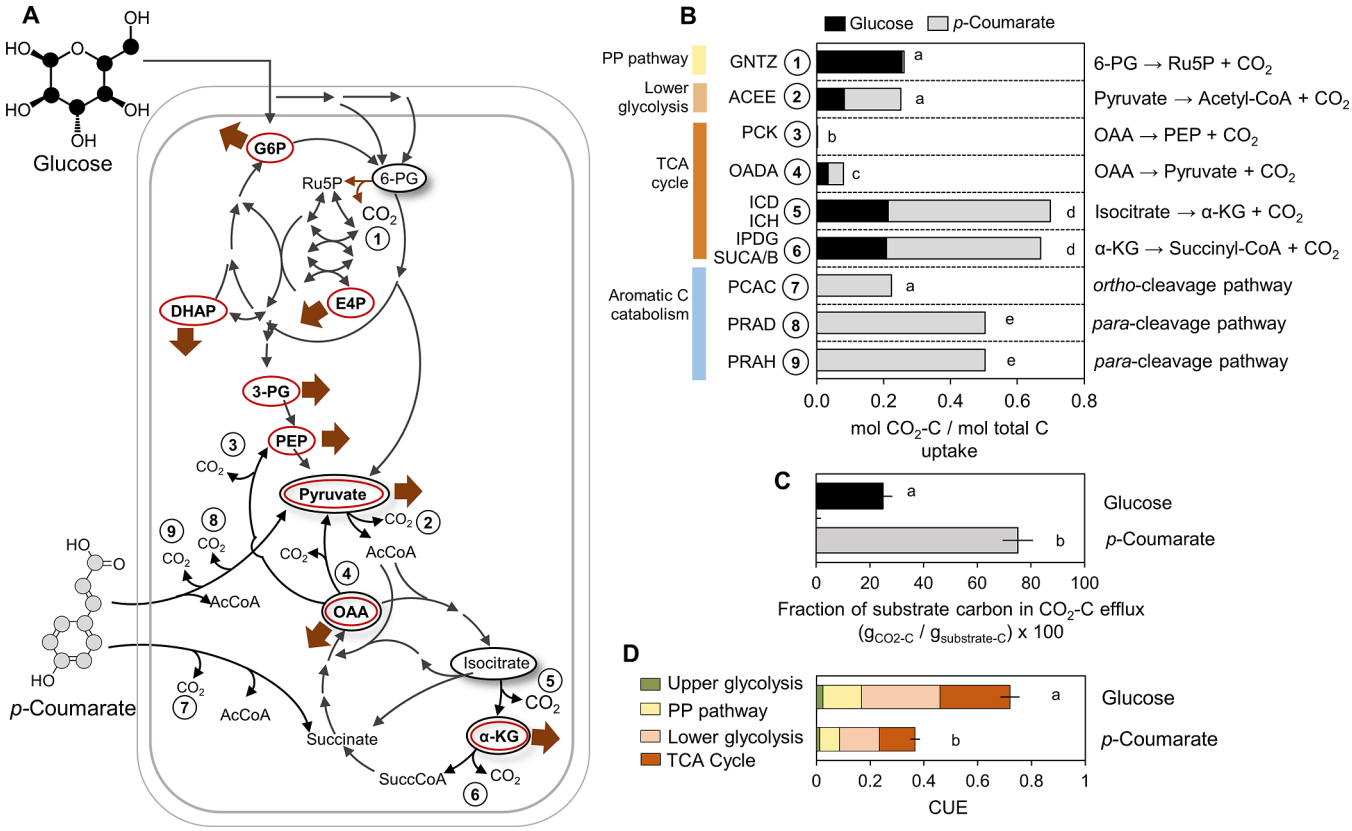

Figure 3. (A) Schematic of the metabolic network in *P. putida* mt-2 with black circles indicating metabolite labeling used to determine substrate contribution in decarboxylation reactions and brown arrows and brown circles indicating flux to biomass synthesis and biomass metabolite precursors, respectively. (B) Contribution of glucose (in black) or *p*-coumarate (in gray) toward CO_2 produced in each decarboxylation reaction in the metabolic network (ratio of CO_2−C efflux rate in mol CO_2−C g_{cdw}^{-1} h^{-1} over total substrate C uptake rate in mol substrate C g_{cdw}^{-1} h^{-1}); the pathway origin for CO_2 efflux from each assimilated substrate is denoted on the left with yellow for the PP pathway, light orange for lower glycolysis, dark orange for the TCA cycle, and blue for aromatic C catabolism. (C) Percent fraction of each assimilated substrate released as CO_2−C: glucose (in black) and *p*-coumarate (in gray). (D) Contribution of metabolic pathways to substrate-dependent CUE calculated from our ^{13}C-metabolic flux analysis of the conversion of the glucose/*p*-coumarate mixture. Metabolite abbreviations in (A and B) are provided in the main text. In (B), the sum of the fractions does not equate to 1 due to carbon retention or recycling in metabolic pathways. In (B, C, and D), error bars represent standard deviation values (n = 3 biological replicates).

GAPA, which is one of the two glyceraldehyde-3-phosphate (GAP) dehydrogenase proteins, was depleted by 2 folds (p-value < 0.01) in the cells grown on the glucose:ferulate mixture compared to glucose alone; the abundance of the other protein (GAPB) remained unchanged in both growth conditions (p-value > 0.392) (Figure 2; Supporting Information Table S4). A functional partitioning of the GAP proteins was reported previously whereby GAPA was implicated to facilitate flux to lower glycolysis, and GAPB was implicated in directing flux in the direction of gluconeogenesis.[48,51] Therefore, from our data, the relatively higher abundance of GAPA in the glucose-only condition compared to the glucose:ferulate mixture was consistent with the importance of GAPA to facilitate glycolysis of glucose (Figure 2). However, despite the relative signifant decrease in GAPA abundance during growth on the substrate mixture compared to glucose alone, our ^{13}C-metabolomics data revealed that the glycolytic flux of glucose-derived carbons downstream of GAP was favored over the gluconeogenic flux of ferulate-derived carbons upstream of 3PG during growth on the mixture with these two substrate types (Figure 1B). These data thus implied that the low GAPA abundance during growth on the mixture was still sufficient to sustain glycolytic flux or that the GAPB can mediate bidirectional reactions at the GAP node whereby the directionality would be driven by the reaction quotient (i.e., relative concentration of product versus reactant). Thus, our ^{13}C metabolomics highight inquires that warrant further investigation of the GAP node.

In sum, given the lack of abundance changes in the majority of the proteins in central carbon metabolism, the proteomics data implied that the flux of aromatic substrate carbons into the CO_2-generating TCA cycle was dictated by carbon input flux into this pathway, which was facilitated by the triggered expression of specific transporter and catabolic proteins for the substrate. Next, we investigated the consequence of the nonuniform metabolic allocation of the sugar and aromatic carbons on their contributions to CO_2 and biomass effluxes.

3.3. Disproportionate CO_2 Efflux from Assimilated Substrate Carbons due to Metabolic Partitioning. To assess quantitatively the consequence of the observed metabolic compartmentalization on CO_2 efflux, we conducted ^{13}C-metabolic flux analysis during feeding on a carbon-equivalent mixture of glucose and *p*-coumarate. First, we determined the distinct contribution of glucose and *p*-coumarate toward CO_2-producing reactions (Figure 3A,B). About 32% of the total normalized CO_2 efflux (per mol of total C uptake) was due to the CO_2-generating reaction in the *ortho*-cleavage and *para*-cleavage pathways during the *p*-coumarate uptake (Figure 3B). Consistent with the exclusive population

https://doi.org/10.1021/acs.est.4c01328
Environ. Sci. Technol. 2024, 58, 11041−11052

of upper glycolysis and the PP pathway by glucose-derived carbons, the decarboxylation reaction of 6-PG to Ru5P in the PP pathway generated CO_2 only from glucose (0.26 ± 0.07 mol of CO_2−C from glucose per mol of total C uptake) (Figure 3A,B). Notably, only four of the nine decarboxylation reactions had contributions from both substrates: the decarboxylation of pyruvate to acetyl-CoA in lower glycolysis (0.08 ± 0.02 mol of CO_2−C from glucose and 0.17 ± 0.02 mol of CO_2−C from *p*-coumarate per mol of total C uptake), the decarboxylation of isocitrate (0.20 ± 0.02 mol of CO_2−C from glucose and 0.46 ± 0.03 mol of CO_2−C from *p*-coumarate per mol of total C uptake), the decarboxylation of α-KG (0.49 ± 0.06 mol of CO_2−C from *p*-coumarate per mol of total C uptake and 0.21 ± 0.03 mol of CO_2−C from glucose per mol of total C uptake), and the anaplerotic reaction of OAA to PEP (0.034 ± 0.01 mol of CO_2−C from glucose and 0.045 ± 0.01 mol of CO_2−C from *p*-coumarate per mol of total C uptake) (Figure 3A,B). Therefore, in accordance with the nonuniform assimilation of each substrate in the TCA cycle metabolites (Figure 3B), more than 69% of the CO_2 generated from both decarboxylation reactions in the TCA cycle (from isocitrate to α-KG and from α-KG to succinate) was derived from *p*-coumarate (*p*-value < 0.02) (Figure 3A,B). In summary, despite the near carbon-equivalent consumption rates for both substrates, only about 25% of the total CO_2 efflux generated during carbon metabolism was derived from glucose, while nearly 75% was from *p*-coumarate (Figure 3C; Supporting Information Tables S5 and S6).

This disproportionate contribution of each substrate to the total CO_2 efflux was accompanied by an unequal contribution of each substrate to the total flux to biomass biosynthesis, as determined by ^{13}C-metabolic flux analysis (Figure 3D; Supporting Information Table S7). This preferential contribution of glucose over *p*-coumarate toward biomass production was due to the aforementioned enrichment of glucose-derived carbons into metabolite precursors to biomass biosynthesis in glycolytic pathways and pathways downstream of glycolysis (Figure 1B,C; Figure 3D). Consequently, the relatively higher glucose investment to biomass resulted in greater ssCUE of glucose (0.72 ± 0.04) and lower ssCUE of *p*-coumarate (0.37 ± 0.06) (*p*-value < 0.02) (Figure 3D). Taken collectively, our data showcased an unequal contribution of the individual lignocellulose-related substrates to CO_2 efflux and biomass due to the unshared metabolic paths of the different substrates, thus resulting in different ssCUEs from the mixture.

To examine further this relationship between substrate-dependent CUE and partitioning in carbon metabolism in other environmental bacteria, we performed ssCUE calculations using reported ^{13}C-metabolic flux analyses of *Bacillus subtilis* 168, *P. putida* KT2440, *Pseudomonas protegens* Pf-5, Sphingobium sp. SYK-6, and Comamonas testosteroni KF-1[36,41,48,52−55] (Figure 4A). For these species widely found in various soil and aquatic ecosystems, the partitioning of carbon fluxes in the metabolic network resulted in 44 to 46% lower ssCUEs during feeding on organic acids and aromatics compared to glucose (Figure 4A). Thus, an unequal contribution to CO_2 efflux and biomass precursors can be predictably explained by the different metabolic paths of the assimilated substrate carbons in several environmentally relevant bacterial species.

3.4. Environmental Implications and Future Considerations. Elucidating microbial processing of organic matter in soils is of critical importance to the understanding of the

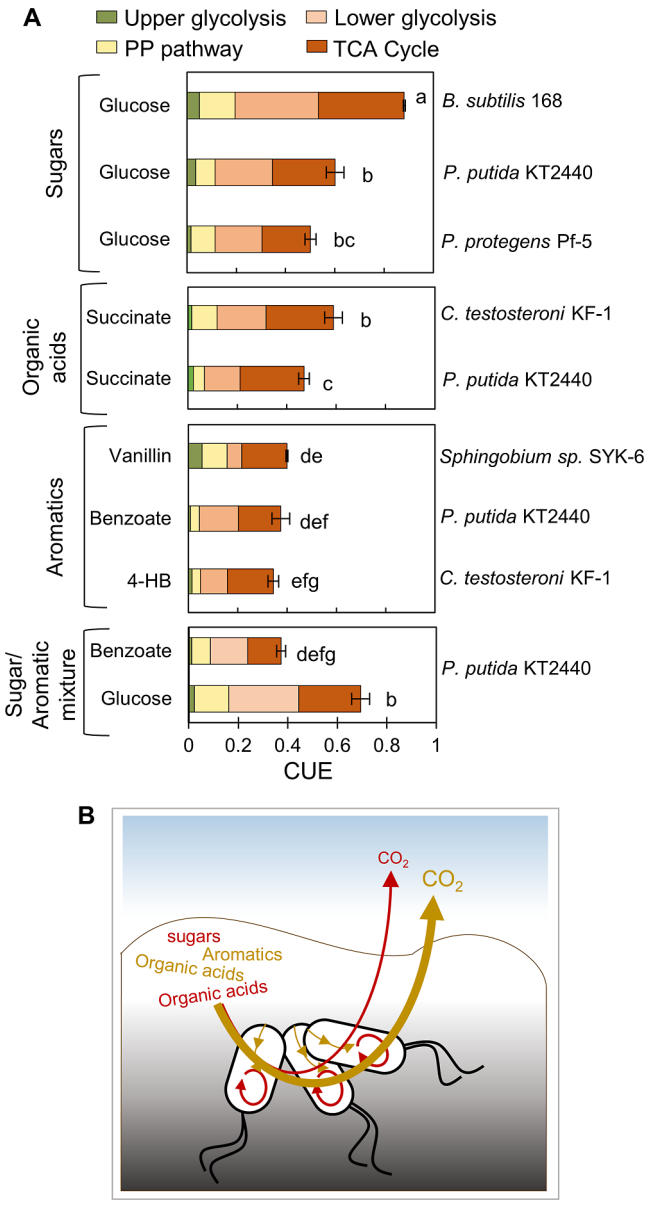

Figure 4. (A) Contribution of different metabolic pathways to ssCUEs calculated based on published metabolic flux analyses for several environmentally relevant bacteria fed on sugars, organic acids, aromatic compounds, or a sugar/aromatic mixture.[36,41,48,52−55] (B) Conceptual overview of the disproportionate contribution of different organic substrates in bioavailable soil organic matter to soil bacterial CUE: fonts and lines in light-brown color indicate glycolytic substrates, glycolytic pathways in the cell, and their resulting contribution to CO_2 efflux; fonts and lines in dark-red color indicate gluconeogenic substrates, TCA cycle pathway in the cells, and their resulting high contribution to CO_2 efflux.

terrestrial CO_2 budget.[1] Based on global-scale data sets and meta-analysis,[56] a negative correlation was proposed between CUE and soil organic carbon loss via microbial CO_2 efflux. Therefore, CUE represents a determining factor in the carbon turnover in soils. Large variations in CUE derived from different organic substrates have been reported[9,11,14,15,57] and the proposed correlation between CUE values and the oxidation state of substrate carbon has not been corroborated by recent studies.[14,15] A fundamental understanding of the relationship of CUE to the metabolism of different substrate

https://doi.org/10.1021/acs.est.4c01328
Environ. Sci. Technol. 2024, 58, 11041−11052

availability is important for the accurate determination of the microbial decomposition of soil organic matter and its ultimate response to projected climate change. Bulk CO_2 measurements are widely used to estimate CUE but information on substrate-specific contribution to CO_2 would require the application of labeled substrates.[19] Still, insights on substrate assimilation into specific metabolic pathways necessitate labeling of biomass derivatives[18] or intracellular metabolites. Here, using ^{13}C-metabolic flux analysis, with a *Pseudomonas* species representing a model soil bacterium with metabolic versatility and adaptability, we resolve the specific metabolic contribution of each substrate in a lignocellulose-related mixture containing glucose and a phenolic acid, toward CO_2 production and biomass synthesis.

Specifically, our algorithm leveraged the contrast in the ^{13}C labeling of metabolites in glycolysis and the PP pathway versus those following aromatic ring cleavage and the TCA cycle to account for fluxes through different decarboxylation reactions in the metabolic network. We revealed a metabolic partitioning whereby nonuniform contribution of each substrate toward biomass and CO_2 resulted in a 3-fold difference in the ssCUE values. This finding is consistent with previous studies, which reported 50% to 3-fold higher CUE for sugars than for short-chain carboxylic acids and aromatic substrates.[9,11,57] Of notable relevance, a recent ^{13}C exometabolomics study of a soil microcosm fed on a diverse mixture of organic substrates revealed different ^{13}C enrichments of metabolites from the assimilated substrates,[58] implying that metabolic partitioning may be a widespread phenomenon in the microbial community. Here, we demonstrated that ssCUEs and CUEs in several environmentally relevant bacteria were also due to distinct partitioning of the substrate carbons in different metabolic pathways, thus demonstrating the broader relevance of our proposed metabolic connection of CUE. We concluded that, in accordance with the relative bioavailability of different organic substrates within soil organic matter, individual substrates processed through the metabolic network would exhibit distinct ssCUE contributions to the overall CUE of soil microorganisms.

In light of our findings, we posit that, on one hand, substrates that are processed through glycolytic and PP pathways, which provide carbon skeletons to DNA and RNA precursors as well as several amino acids for protein synthesis, would result in a high CUE; on the other hand, there would be a relatively lower CUE for aromatic substrates and other gluconeogenic substrates such as short-chain carboxylic acids that feed directly into the TCA cycle, which generates a high flux through CO_2-producting reactions in addition to providing metabolite precursors to protein biosynthesis (Figure 4B). Consistent with our data, a previous study[18] reported a negative correlation between CUE calculation and the relative investment of assimilated ^{13}C-glucose into TCA cycle flux based on positional ^{13}C labeling into phospholipid fatty acids in soil microbes. Here, we further expanded on this metabolism-guided perspective to demonstrate explicitly that the contributions of ssCUE from a mixture to CUE were due to specific allocation of carbons for each substrate into different metabolic pathways with a varying extent of CO_2-generating reactions.

To apply broadly this metabolic approach to ssCUE predictions, there are several considerations regarding the complexity of environmental matrices that need to be addressed in future research. First, bioavailable substrates in soil organic matter represent a diverse group of substrates of differing chemistry and structure, including various carbohydrates and organic acids.[20,59] Here, we determined that the distinct metabolic paths of assimilated sugar versus an assimilated lignin-related aromatic compound resulted in dissimilar ssCUEs, in agreement with different soil microbial CUEs reported for different types of organic substrates.[9,11,14] Subsequent studies will need to address the metabolic flux network of a heterogeneous mixture of bioavailable organic compounds with respect to how microorganisms prioritize anabolism (i.e., biomass growth) versus catabolism (i.e., metabolic conversion and CO_2 generation) in soils,[60] by building on the approach highlighted by Wu et al.[18] and incorporating the ^{13}C-metabolomics approach shown here. Second, the present study was conducted in an aerobic environment with nonlimiting concentrations of inorganic nutrients, such as nitrogen, iron, phosphorus, and trace metals. It was shown that iron availability can lead to selective carbon assimilation in Pseudomonas species.[35] Furthermore, ^{13}C-exometabolomics profiling has captured specific metabolic pathways in soil samples in response to different redox conditions.[61] The availability of nitrogen or phosphorus and environmental cues such as temperature and moisture can influence microbial carbon utilization.[9,14,17,62,63] How these environmental factors would modulate the metabolic strategies deployed by soil microorganisms remains to be investigated.[62,63] Third, based both on genome-predicted metabolic models and field-scale experimental observations, it was determined that differences in CUE values are both taxon-specific and genus-specific.[64,65] Soil microbial communities encompass a diverse assembly of bacteria and fungi with variable metabolic capabilities for different bioavailable substrates.[3,66,67] In fact, microbial diversity was shown to be a determining factor in establishing CUE in soil.[68] Different rates of TCA cycle fluxes normalized to substrate uptake flux were observed for Gram-positive bacteria versus Gram-negative bacteria, based on incorporation of ^{13}C-sugar carbons into fatty acids.[18] How these differences in TCA cycle and other pathway activities would be manifested for a mixture of substrate carbons was not investigated. Building on our findings, implementing the routing of different bioavailable substrate carbons through the CO_2-producing reactions involved in variable metabolic network fluxes in different microbial taxa will be necessary to capture microbial heterogeneity in soil carbon budgets.

■ ASSOCIATED CONTENT

Supporting Information

The Supporting Information is available free of charge at https://pubs.acs.org/doi/10.1021/acs.est.4c01328.

Data sets from metabolomics experiments, proteomics experiments, and metabolic flux analysis (PDF)

■ AUTHOR INFORMATION

Corresponding Author

Ludmilla Aristilde − *Department of Biological and Environmental Engineering, College of Agriculture and Life Sciences, Cornell University, Ithaca, New York 14853, United States; Department of Civil and Environmental Engineering, McCormick School of Engineering and Applied Science, Northwestern University, Evanston, Illinois 60208, United*

https://doi.org/10.1021/acs.est.4c01328
Environ. Sci. Technol. 2024, 58, 11041−11052

States; orcid.org/0000-0002-8566-1486; Phone: 847-491-2999; Email: ludmilla.aristilde@northwestern.edu

Authors

Caroll M. Mendonca − *Department of Biological and Environmental Engineering, College of Agriculture and Life Sciences, Cornell University, Ithaca, New York 14853, United States; Department of Civil and Environmental Engineering, McCormick School of Engineering and Applied Science, Northwestern University, Evanston, Illinois 60208, United States*

Lichun Zhang − *Department of the Geophysical Sciences, University of Chicago, Chicago, Illinois 60637, United States*

Jacob R. Waldbauer − *Department of the Geophysical Sciences, University of Chicago, Chicago, Illinois 60637, United States;* orcid.org/0000-0002-0338-6143

Complete contact information is available at: https://pubs.acs.org/10.1021/acs.est.4c01328

Notes

The authors declare no competing financial interest.

■ ACKNOWLEDGMENTS

Research funding was from the U.S. National Science Foundation (CBET-1653092; CBET-2041669; CBET-2022854) and Northwestern University. We thank three anonymous reviewers for their insightful comments.

■ REFERENCES

(1) Gougoulias, C.; Clark, J. M.; Shaw, L. J. The role of soil microbes in the global carbon cycle: tracking the below-ground microbial processing of plant-derived carbon for manipulating carbon dynamics in agricultural systems. *J. Sci. Food Agric.* **2014**, *94*, 2362−2371.

(2) Ali, R. S.; Poll, C.; Kandeler, E. Soil Properties Control Microbial Carbon Assimilation and Its Mean Residence Time. *Front. Environ. Sci.* **2020**, *8*, 33.

(3) Kramer, S.; Dibbern, D.; Moll, J.; Huenninghaus, M.; Koller, R.; Krueger, D.; Marhan, S.; Urich, T.; Wubet, T.; Bonkowski, M.; Buscot, F.; Lueders, T.; Kandeler, E. Resource partitioning between bacteria, fungi, and protists in the detritusphere of an agricultural soil. *Front. Microbiol.* **2016**, *7*, 1524.

(4) Sun, W.; Sun, X.; Häggblom, M. M.; Kolton, M.; Lan, L.; Li, B.; Dong, Y.; Xu, R.; Li, F. Identification of Antimonate Reducing Bacteria and Their Potential Metabolic Traits by the Combination of Stable Isotope Probing and Metagenomic-Pangenomic Analysis. *Environ. Sci. Technol.* **2021**, *55*, 13902−13912.

(5) Barnett, S. E.; Youngblut, N. D.; Koechli, C. N.; Buckley, D. H. Multisubstrate DNA stable isotope probing reveals guild structure of bacteria that mediate soil carbon cycling. *Proc. Natl. Acad. Sci. U.S.A.* **2021**, *118*, 1−11.

(6) Schimel, J.; Weintraub, M. N.; Moorhead, D. Estimating microbial carbon use efficiency in soil: Isotope-based and enzyme-based methods measure fundamentally different aspects of microbial resource use. *Soil Biol. Biochem.* **2022**, *169*, 108677.

(7) Geyer, K. M.; Kyker-Snowman, E.; Grandy, A. S.; Frey, S. D. Microbial carbon use efficiency: accounting for population, community, and ecosystem-scale controls over the fate of metabolized organic matter. *Biogeochemistry* **2016**, *127*, 173−188.

(8) Pold, G.; Domeignoz-Horta, L. A.; Morrison, E. W.; Frey, S. D.; Sistla, S. A.; DeAngelis, K. M. Carbon use efficiency and its temperature sensitivity covary in soil bacteria. *mBio* **2020**, *11*, 1−16.

(9) Qiao, Y.; Wang, J.; Liang, G.; Du, Z.; Zhou, J.; Zhu, C.; Huang, K.; Zhou, X.; Luo, Y.; Yan, L.; Xia, J. Global variation of soil microbial carbon-use efficiency in relation to growth temperature and substrate supply. *Sci. Rep.* **2019**, *9*, 5621−5628.

(10) Manzoni, S.; Taylor, P.; Richter, A.; Porporato, A.; Ågren, G. I. Environmental and stoichiometric controls on microbial carbon-use efficiency in soils. *New Phytol.* **2012**, *196*, 79−91.

(11) Sugai, S. F.; Schimel, J. P. Decomposition and biomass incorporation of 14C-labeled glucose and phenolics in taiga forest floor: effect of substrate quality, successional state, and season. *Soil Biol. Biochem.* **1993**, *25*, 1379−1389.

(12) LaRowe, D. E.; Van Cappellen, P. Degradation of natural organic matter: A thermodynamic analysis. *Geochim. Cosmochim. Acta* **2011**, *75*, 2030−2042.

(13) Kleber, M. What is recalcitrant soil organic matter? *Environ. Chem.* **2010**, *7*, 320−332.

(14) Islam, M. R.; Singh, B.; Dijkstra, F. A. Microbial carbon use efficiency of glucose varies with soil clay content: A meta-analysis. *Appl. Soil Ecol.* **2023**, *181*, 104636.

(15) Cyle, K. T.; Klein, A. R.; Aristilde, L.; Martínez, C. E. Dynamic utilization of low-molecular-weight organic substrates across a microbial growth rate gradient. *J. Appl. Microbiol.* **2022**, *133*, 1479−1495.

(16) Park, J. O.; Liu, N.; Holinski, K. M.; Emerson, D. F.; Qiao, K.; Woolston, B. M.; Xu, J.; Lazar, Z.; Islam, M. A.; Vidoudez, C.; Girguis, P. R.; Stephanopoulos, G. Synergistic substrate cofeeding stimulates reductive metabolism. *Nat. Metab.* **2019**, *1*, 643−651.

(17) Brown, R. W.; Chadwick, D. R.; Bending, G. D.; Collins, C. D.; Whelton, H. L.; Daulton, E.; Covington, J. A.; Bull, I. D.; Jones, D. L. Nutrient (C, N and P) enrichment induces significant changes in the soil metabolite profile and microbial carbon partitioning. *Soil Biol. Biochem.* **2022**, *172*, 108779.

(18) Wu, W.; Dijkstra, P.; Hungate, B. A.; Shi, L.; Dippold, M. A. In situ diversity of metabolism and carbon use efficiency among soil bacteria. *Sci. Adv.* **2022**, *8*, 3958.

(19) Dijkstra, P.; Blankinship, J. C.; Selmants, P. C.; Hart, S. C.; Koch, G. W.; Schwartz, E.; Hungate, B. A. Probing carbon flux patterns through soil microbial metabolic networks using parallel position-specific tracer labeling. *Soil Biol. Biochem.* **2011**, *43*, 126−132.

(20) Angst, G.; Mueller, K. E.; Nierop, K. G. J.; Simpson, M. J. Plant- or microbial-derived? A review on the molecular composition of stabilized soil organic matter. *Soil Biol. Biochem.* **2021**, *156*, 108189.

(21) Chen, H. Chemical Composition and Structure of Natural Lignocellulose. In *Biotechnology of Lignocellulose*; Springer: Netherlands, 2014; pp 25−71.

(22) Xu, F.; Li, Y. Encyclopedia of Sustainable Technologies. In *Biomass Digestion*; Elsevier, 2017; pp 197−204..

(23) Ruiz-Dueñas, F. J.; Martínez, Á. T. Microbial degradation of lignin: how a bulky recalcitrant polymer is efficiently recycled in nature and how we can take advantage of this. *Microb. Biotechnol.* **2009**, *2*, 164−177.

(24) Magdoff, F.; Van Es, H. *Building Soils for Better Crops*, 2nd ed.; Sustainable Agriculture Network, 2001.

(25) del Cerro, C.; Erickson, E.; Dong, T.; Wong, A. R.; Eder, E. K.; Purvine, S. O.; Mitchell, H. D.; Weitz, K. K.; Markillie, L. M.; Burnet, M. C.; Hoyt, D. W.; Chu, R. K.; Cheng, J. F.; Ramirez, K. J.; Katahira, R.; Xiong, W.; Himmel, M. E.; Subramanian, V.; Linger, J. G.; Salvachúa, D.; Salvachúa, D. Intracellular pathways for lignin catabolism in white-rot fungi. *Proc. Natl. Acad. Sci. U.S.A.* **2021**, *118*, No. e2017381118.

(26) Bi, R.; Lawoko, M.; Henriksson, G. *Phoma herbarum*, a soil fungus able to grow on natural lignin and synthetic lignin (DHP) as sole carbon source and cause lignin degradation. *J. Ind. Microbiol. Biotechnol.* **2016**, *43*, 1175−1182.

(27) Salih, N. K. M.; Jusuf, N. H.; Hamid, A. A.; Yusoff, W. M. W. High prevalence of *Pseudomonas* species in soil samples from Ternate Island-Indonesia. *Pak. J. Biol. Sci.* **2009**, *12*, 1036−1040.

(28) Duponnois, R.; Kisa, M.; Assigbetse, K.; Prin, Y.; Thioulouse, J.; Issartel, M.; Moulin, P.; Lepage, M. Fluorescent pseudomonads occurring in *Macrotermes subhyalinus* mound structures decrease Cd toxicity and improve its accumulation in sorghum plants. *Sci. Total Environ.* **2006**, *370*, 391−400.

(29) Becker, J.; Wittmann, C. A field of dreams: Lignin valorization into chemicals, materials, fuels, and health-care products. *Biotechnol. Adv.* **2019**, *37*, 107360.
(30) Salvachúa, D.; Karp, E. M.; Nimlos, C. T.; Vardon, D. R.; Beckham, G. T. Towards lignin consolidated bioprocessing: simultaneous lignin depolymerization and product generation by bacteria. *Green Chem.* **2015**, *17*, 4951−4967.
(31) Díaz Rodríguez, C. A.; Díaz-García, L.; Bunk, B.; Spröer, C.; Herrera, K.; Tarazona, N. A.; Rodriguez-R, L. M.; Overmann, J.; Jiménez, D. J. Novel bacterial taxa in a minimal lignocellulolytic consortium and their potential for lignin and plastics transformation. *ISME Commun.* **2022**, *2* (1), 89.
(32) Hefni, M. E.; Amann, L. S.; Witthöft, C. M. A HPLC-UV Method for the Quantification of Phenolic Acids in Cereals. *Food Anal. Methods* **2019**, *12*, 2802−2812.
(33) Barzen-Hanson, K. A.; Wilkes, R. A.; Aristilde, L. Quantitation of carbohydrate monomers and dimers by liquid chromatography coupled with high-resolution mass spectrometry. *Carbohydr. Res.* **2018**, *468*, 30−35.
(34) Melamud, E.; Vastag, L.; Rabinowitz, J. D. Metabolomic Analysis and Visualization Engine for LC−MS Data. *Anal. Chem.* **2010**, *82*, 9818−9826.
(35) Mendonca, C. M.; Yoshitake, S.; Wei, H.; Werner, A.; Sasnow, S. S.; Thannhauser, T. W.; Aristilde, L. Hierarchical routing in carbon metabolism favors iron-scavenging strategy in iron-deficient soil *Pseudomonas* species. *Proc. Natl. Acad. Sci. U.S.A.* **2020**, *117* (51), 32358−32369.
(36) Kukurugya, M. A.; Mendonca, C. M.; Solhtalab, M.; Wilkes, R. A.; Thannhauser, T. W.; Aristilde, L. Multi-omics analysis unravels a segregated metabolic flux network that tunes co-utilization of sugar and aromatic carbons in *Pseudomonas putida*. *J. Biol. Chem.* **2019**, *294*, 8464−8479.
(37) Weitzel, M.; Nöh, K.; Dalman, T.; Niedenführ, S.; Stute, B.; Wiechert, W. 13CFLUX2−high-performance software suite for (13)C-metabolic flux analysis. *Bioinformatics* **2013**, *29*, 143−145.
(38) Greated, A.; Lambertsen, L.; Williams, P. A.; Thomas, C. M. Complete sequence of the IncP-9 TOL plasmid pWW0 from Pseudomonas putida. *Environ. Microbiol.* **2002**, *4*, 856−871.
(39) Timmis, K. N. *Pseudomonas putida*: a cosmopolitan opportunist par excellence. *Environ. Microbiol.* **2002**, *4*, 779−781.
(40) van Duuren, J. B. J. H.; Puchałka, J.; Mars, A. E.; Bücker, R.; Eggink, G.; Wittmann, C.; dos Santos, V. A. M.; Dos Santos, V. A. Reconciling in vivo and in silico key biological parameters of *Pseudomonas putida* KT2440 during growth on glucose under carbon-limited condition. *BMC Biotechnol.* **2013**, *13*, 93.
(41) Sasnow, S. S.; Wei, H.; Aristilde, L. Bypasses in intracellular glucose metabolism in iron-limited *Pseudomonas putida*. *Microbiologyopen* **2016**, *5*, 3−20.
(42) Zamboni, N.; Fendt, S.-M.; Rühl, M.; Sauer, U. 13C-based metabolic flux analysis. *Nat. Protoc.* **2009**, *4*, 878−892.
(43) Buescher, J. M.; Antoniewicz, M. R.; Boros, L. G.; Burgess, S. C.; Brunengraber, H.; Clish, C. B.; DeBerardinis, R. J.; Feron, O.; Frezza, C.; Ghesquiere, B.; Gottlieb, E.; Hiller, K.; Jones, R. G.; Kamphorst, J. J.; Kibbey, R. G.; Kimmelman, A. C.; Locasale, J. W.; Lunt, S. Y.; Maddocks, O. D.; Malloy, C.; Metallo, C. M.; Meuillet, E. J.; Munger, J.; Nöh, K.; Rabinowitz, J. D.; Ralser, M.; Sauer, U.; Stephanopoulos, G.; St-Pierre, J.; Tennant, D. A.; Wittmann, C.; Vander Heiden, M. G.; Vazquez, A.; Vousden, K.; Young, J. D.; Zamboni, N.; Fendt, S. M. A roadmap for interpreting 13C metabolite labeling patterns from cells. *Curr. Opin. Biotechnol.* **2015**, *34*, 189−201.
(44) Erde, J.; Loo, R. R. O.; Loo, J. A. Enhanced FASP (eFASP) to Increase Proteome Coverage and Sample Recovery for Quantitative Proteomic Experiments. *J. Proteome Res.* **2014**, *13*, 1885−1895.
(45) Waldbauer, J.; Zhang, L.; Rizzo, A.; Muratore, D. diDO-IPTL: A Peptide-Labeling Strategy for Precision Quantitative Proteomics. *Anal. Chem.* **2017**, *89*, 11498−11504.
(46) Benjamini, Y.; Hochberg, Y. Controlling the False Discovery Rate: A Practical and Powerful Approach to Multiple Testing. *J R Stat Soc Series B: Methodol.* **1995**, *57*, 289−300.
(47) Nikel, P. I.; Chavarría, M.; Fuhrer, T.; Sauer, U.; de LorenzoLorenzo, V. V. *Pseudomonas putida* KT2440 strain metabolizes glucose through a cycle formed by enzymes of the Entner-Doudoroff, embden-meyerhof-parnas, and pentose phosphate pathways. *J. Biol. Chem.* **2015**, *290*, 25920−25932.
(48) Wilkes, R. A.; Waldbauer, J.; Aristilde, L. Analogous Metabolic Decoupling in *Pseudomonas putida* and *Comamonas testosteroni* Implies Energetic Bypass to Facilitate Gluconeogenic Growth. *mBio* **2021**, *12*, No. e03259−21.
(49) Franklin, F. C. H.; Bagdasarian, M.; Bagdasarian, M. M.; Timmis, K. N. Molecular and functional analysis of the TOL plasmid pWWO from *Pseudomonas putida* and cloning of genes for the entire regulated aromatic ring meta cleavage pathway. *Proc. Natl. Acad. Sci. U.S.A.* **1981**, *78*, 7458−7462.
(50) Worsey, M. J.; Williams, P. A. Metabolism of toluene and xylenes by *Pseudomonas (putida (arvilla)* mt-2: evidence for a new function of the TOL plasmid. *J. Bacteriol.* **1975**, *124*, 7−13.
(51) Buffing, M. F.; Link, H.; Christodoulou, D.; Sauer, U. Capacity for instantaneous catabolism of preferred and non-preferred carbon sources in *Escherichia coli* and *Bacillus subtilis*. *Sci. Rep.* **2018**, *8*, 11760.
(52) Wilkes, R. A.; Mendonca, C. M.; Aristilde, L. A Cyclic Metabolic Network in *Pseudomonas protegens* Pf-5 Prioritizes the Entner-Doudoroff Pathway and Exhibits Substrate Hierarchy during Carbohydrate Co-Utilization. *Appl. Environ. Microbiol.* **2019**, *85*, No. e02084−18.
(53) Wilkes, R. A.; Waldbauer, J.; Carroll, A.; Nieto-Domínguez, M.; Parker, D. J.; Zhang, L.; Guss, A. M.; Aristilde, L. Complex regulation in a Comamonas platform for diverse aromatic carbon metabolism. *Nat. Chem. Biol.* **2023**, *19*, 651−662.
(54) Schilling, O.; Frick, O.; Herzberg, C.; Ehrenreich, A.; Heinzle, E.; Wittmann, C.; Stülke, J. Transcriptional and Metabolic Responses of Bacillus subtilis to the Availability of Organic Acids: Transcription Regulation Is Important but Not Sufficient To Account for Metabolic Adaptation. *Appl. Environ. Microbiol.* **2007**, *73*, 499−507.
(55) Varman, A. M.; He, L.; Follenfant, R.; Wu, W.; Wemmer, S.; Wrobel, S. A.; Tang, Y. J.; Singh, S. Decoding how a soil bacterium extracts building blocks and metabolic energy from ligninolysis provides road map for lignin valorization. *Proc. Natl. Acad. Sci. U.S.A.* **2016**, *113*, E5802−E5811.
(56) Tao, F.; Huang, Y.; Hungate, B. A.; Manzoni, S.; Frey, S. D.; Schmidt, M. W. I.; Reichstein, M.; Carvalhais, N.; Ciais, P.; Jiang, L.; Lehmann, J.; Wang, Y. P.; Houlton, B. Z.; Ahrens, B.; Mishra, U.; Hugelius, G.; Hocking, T. D.; Lu, X.; Shi, Z.; Viatkin, K.; Vargas, R.; Yigini, Y.; Omuto, C.; Malik, A. A.; Peralta, G.; Cuevas-Corona, R.; Di Paolo, L. E.; Luotto, I.; Liao, C.; Liang, Y. S.; Saynes, V. S.; Huang, X.; Luo, Y. Microbial carbon use efficiency promotes global soil carbon storage. *Nature* **2023**, *618*, 981−985.
(57) Adingo, S.; Yu, J. R.; Xuelu, L.; Li, X.; Jing, S.; Xiaong, Z. Variation of soil microbial carbon use efficiency (CUE) and its Influence mechanism in the context of global environmental change: a review. *PeerJ* **2021**, *9*, No. e12131.
(58) Wilhelm, R. C.; Barnett, S. E.; Swenson, T. L.; Youngblut, N. D.; Koechli, C. N.; Bowen, B. P.; Northen, T. R.; Buckley, D. H. Tracing Carbon Metabolism with Stable Isotope Metabolomics Reveals the Legacy of Diverse Carbon Sources in Soil. *Appl. Environ. Microbiol.* **2022**, *88*, No. e00839−22.
(59) Fischer, H.; Meyer, A.; Fischer, K.; Kuzyakov, Y. Carbohydrate and amino acid composition of dissolved organic matter leached from soil. *Soil Biol. Biochem.* **2007**, *39*, 2926−2935.
(60) Gan, S.; Guo, P.; Wu, Y.; Zhao, Y. A Novel Method for Unraveling the Black Box of Dissolved Organic Matter in Soils by FT-ICR-MS Coupled with Induction-Based Nanospray Ionization. *Environ. Sci. Technol. Lett.* **2021**, *8*, 356−361.
(61) Hassanpour, B.; Aristilde, L. Redox-Related Metabolic Dynamics Imprinted on Short-Chain Carboxylic Acids in Soil Water

Extracts: A 13C-Exometabolomics Analysis. *Environ. Sci. Technol. Lett.* **2021**, *8*, 183−191.
(62) Zheng, Q.; Hu, Y.; Zhang, S.; Noll, L.; Böckle, T.; Richter, A.; Wanek, W. Growth explains microbial carbon use efficiency across soils differing in land use and geology. *Soil Biol. Biochem.* **2019**, *128*, 45−55.
(63) Garayburu-Caruso, V. A.; Stegen, J. C.; Song, H.-S.; Renteria, L.; Wells, J.; Garcia, W.; Resch, C. T.; Goldman, A.; Chu, R.; Toyoda, J.; Graham, E. B. Carbon Limitation Leads to Thermodynamic Regulation of Aerobic Metabolism. *Environ. Sci. Technol. Lett.* **2020**, *7*, 517−524.
(64) Saifuddin, M.; Bhatnagar, J. M.; Segrè, D.; Finzi, A. C. Microbial carbon use efficiency predicted from genome-scale metabolic models. *Nat. Commun.* **2019**, *10*, 3568.
(65) Pold, G.; Sistla, S. A.; Deangelis, K. M. Metabolic tradeoffs and heterogeneity in microbial responses to temperature determine the fate of litter carbon in simulations of a warmer world. *Biogeosciences* **2019**, *16*, 4875−4888.
(66) Leff, J. W.; Jones, S. E.; Prober, S. M.; Barberán, A.; Borer, E. T.; Firn, J. L.; Harpole, W. S.; Hobbie, S. E.; Hofmockel, K. S.; Knops, J. M.; McCulley, R. L.; La Pierre, K.; Risch, A. C.; Seabloom, E. W.; Schütz, M.; Steenbock, C.; Stevens, C. J.; Fierer, N. Consistent responses of soil microbial communities to elevated nutrient inputs in grasslands across the globe. *Proc. Natl. Acad. Sci. U.S.A.* **2015**, *112*, 10967−10972.
(67) Lang, M.; Zou, W.; Chen, X.; Zou, C.; Zhang, W.; Deng, Y.; Zhu, F.; Yu, P.; Chen, X. Soil Microbial Composition and phoD Gene Abundance Are Sensitive to Phosphorus Level in a Long-Term Wheat-Maize Crop System. *Front. Microbiol.* **2021**, *11*, 3547.
(68) Dang, C.; Morrissey, E. M. The size and diversity of microbes determine carbon use efficiency in soil. *Environ Microbiol.* **2024**, *26*, No. e16633.

https://doi.org/10.1021/acs.est.4c01328
Environ. Sci. Technol. 2024, 58, 11041−11052